Chapter 4

Results & Discussion

Section (A)

Characterization of PVA/CuI Polymer Electrolytes

4.A.1 X-Ray Diffraction Investigation

Fig.(4.1) shows XRD pattern of polymer electrolyte layers of different composition. A broad peak at 19.12° has been observed in Fig.(4.1a), which was assigned to OH semicrystalline phase originated from PVA. However, in the complexed system Fig.(4.1b–g), the pure PVA peak (19.12°) was increased in broadness and decreased in intensity by adding the salt with a different ratio of C=NaI/$CuCl_2$. This increase in broadness of the peak reveals the amorphous nature of the complexed system. These results can be interpreted in terms of Hodge et al.[67] criterion which has established a correlation between the height of the peak and the degree of crystallinity. Fig.(4.1b) shows new sharp peaks raised at 25.49°, 42.24° and 49.99° indicating the growth of CuI crystallites in the polymer matrix. These peaks appeared until the ratio C reached 5 then the observed peaks disappear, which indicating the increase of the amorphisity of the polymer electrolyte.

Also typical XRD patterns for the powder extracted from polymer colloidal using centrifuge shown in Fig.(4.2), it shows three diffraction peaks at 25.28°, 42.08°and 49.76°corresponding to the (0 1 2), (1 1 0) and (2 0 2) planes of CuI crystals which could be indexed to hexagonal structure (the lattice constants are, a = 4.291 A° and c = 21.48 A°), which were consistent with the literature data of JCPDS 83-1145.

The average particle size can be calculated using the first sphere approximation of Debye–Scherrer formula [68],

$$D = \frac{0.9\lambda}{B\cos\theta} \qquad (4.1)$$

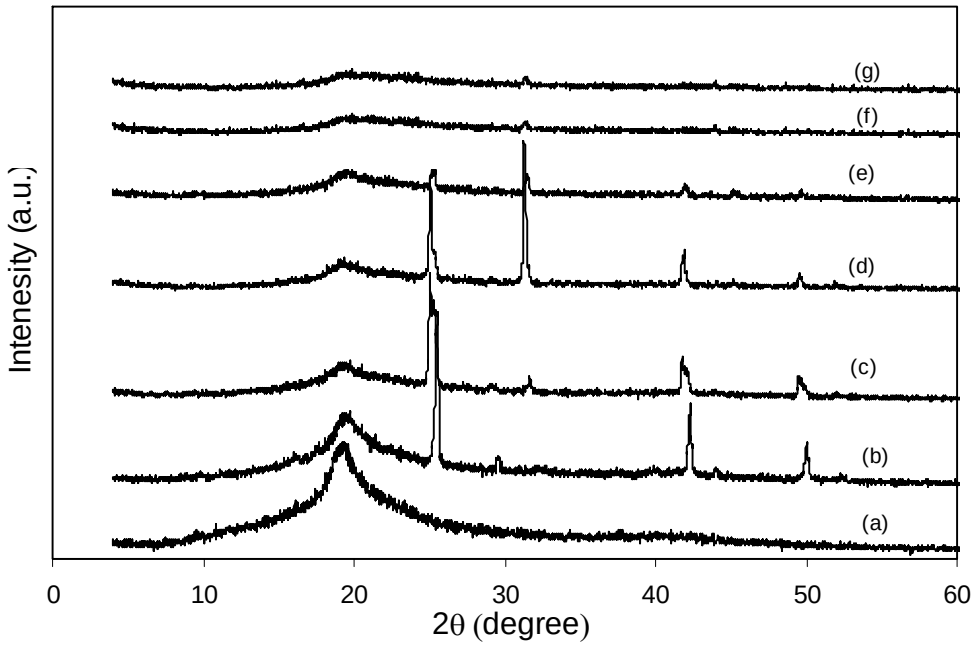

Fig.(4.1): X-ray diffraction pattern for (a) C=0, (b) C=1.66, (c) C=3.33, (d) C=5, (e) C= 6.67, (f) C=8.33 & (g) C=10 polymer electrolyte films.

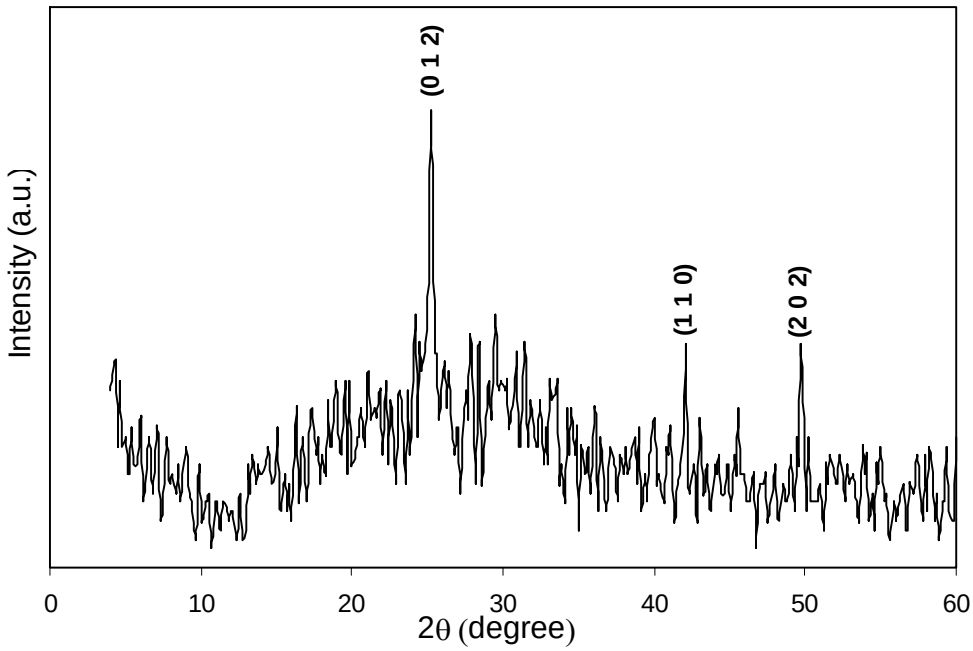

Fig.(4.2): X-ray diffraction pattern of nanoparticles precipitate from polymer electrolyte solution.

Table (4.1): Extracted values of the average Particle size of CuI nanoParticle for polymer electrolyte samples.

C ratio ($NaI/CuCl_2$)	Particle size (nm)
0	-
1.66	36
3.33	15
5	57
6.67	23
8.33	56
10	55

where D is the average diameter of the crystals, λ is the wavelength of X-ray radiation, B is the full width at half maximum intensity of the peak and θ is the incident angle. The average particle size of CuI nanoparticles is equal to ~ 55 nm extracted by centrifuge where the particle size of CuI embedded in polymer electrolyte obtained at different mentioned C ratio are shown in table (4.1). These values of CuI particle sizes lie in the same range of those of precipitates 55 nm. The apparent fluctuation of the particle size of CuI phase may be attributed to the particles aggregation and/or complexation of NaI in PVA polymer matrix.

4.A.2 Scanning Electron Microscopy

Scanning electron microscopy has been used to study the compatibility between various components of the polymer electrolytes through the detection of phase separations and interfaces. Fig.(4.3) shows the SEM photograph of polymer electrolyte films. The films exhibit little density of grain distribution at surface morphology. It can be seen from the images that the grain aggregates with increasing C ratio. It can also be seen that some tiny pores existed between the filler–polymer interfaces which can be attributed to the compatibility between the filler and the polymer. The surface morphology of the PVA/CuI polymer electrolyte films shows many aggregates or chunks randomly distributed on the top surface. It was found that the dimension of those aggregates embedded in the PVA matrix lie in the range 1- 2μm. These results indicate that the nano-sized CuI particles tended to form aggregates and dispersed into the PVA polymer matrix.

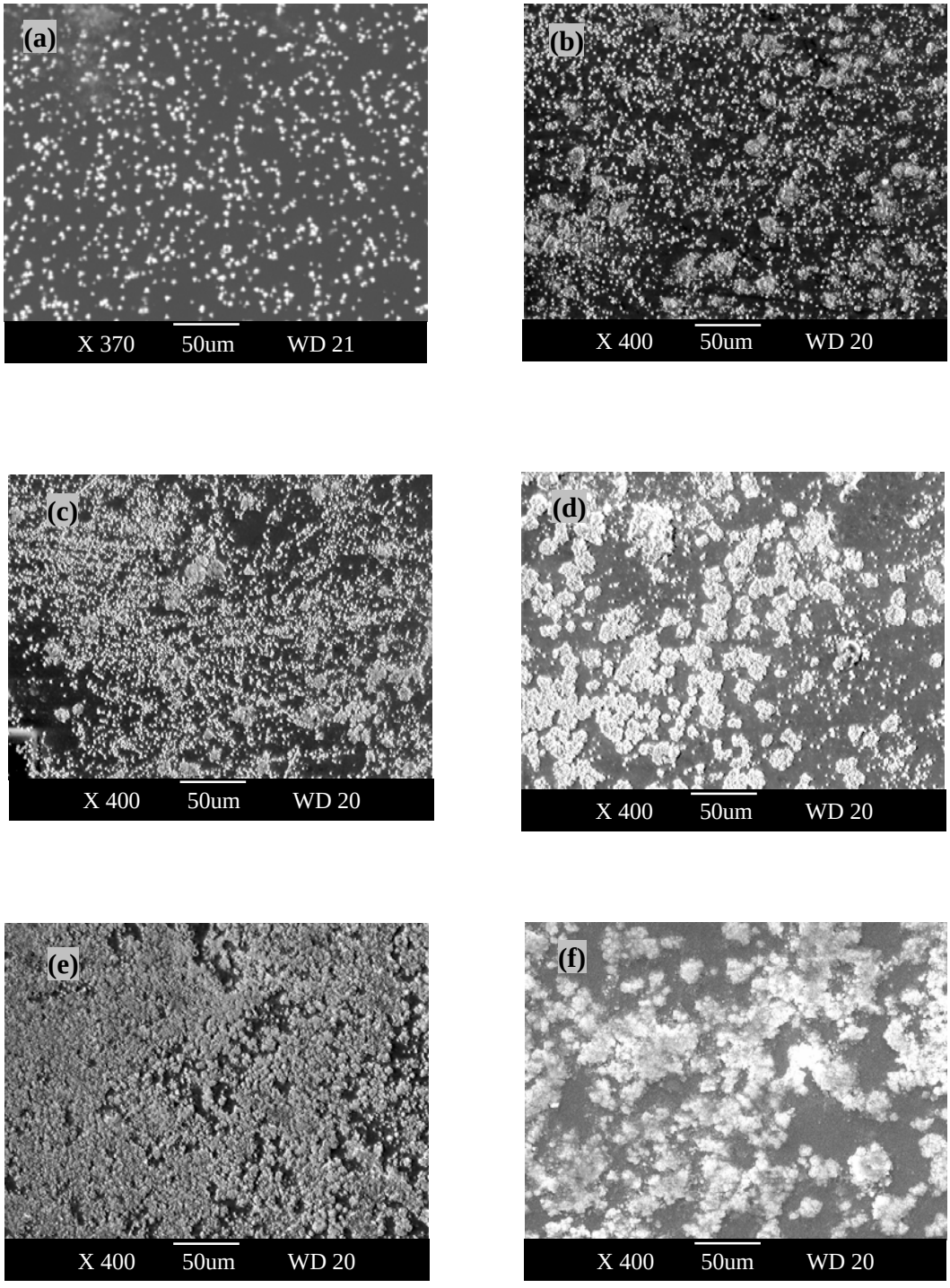

Fig.(4.3): SEM images of polymer electrolyte at different NaI/$CuCl_2$ ratio C, (a) C=1.66 (b) C=3.33, (c) C=5, (d) C= 6.67, (e) C=8.33 & (f) C=10.

4.A.3 Thermogravimetric Analysis (TGA)

TGA is considered as the most important method for studying thermal stability of polymers. Moreover, the kinetics of the accompanied decomposition reaction has been reviewed. The sample weight decreases slowly as the reaction begins, then decreases rapidly over a comparatively narrow temperature range and finally levels off as the reactants are used up. The shape of the curve depends primarily upon the kinetics parameters involved, i.e. order of reaction (n) and activation energy (E). The values of these parameters are important in estimation of thermal stability. TGA is used in studying the samples in the temperature range of 30–400 °C. Fig.(4.4) shows typical TGA thermograms of weight loss as a function of temperature for the PVA electrolyte having a different ratio of NaI/$CuCl_2$. The general behavior shows two main degradation stages. It is evident that initial weight loss up to 100 °C is closely associated with the loss of absorbed water molecules (dehydration). The second weight loss occurs between 230 and 350 °C for all samples with maximum weight loss rate at certain temperatures. The characteristic temperature is extracted using the differentiation of the data obtained, see the differentiation curve Fig.(4.4), and summarized in table (4.2). In addition the first TGA onset temperature was corresponding to water dehydration while the second onset temperature in the range 230 to 350 °C corresponds to polymer decomposition, and those two onset temperatures were calculated and summarized in table (4.2). The temperature at maximum loss rate varies between 275 and 323 °C, it depends on the salt complex with polymer matrix. Also, area under the curve has been calculated form 30 to 400 °C for all the samples and given in table (4.2), this area represents the total heat capacitance for the sample.

The thermal decomposition of the solid can be expressed by the following reaction rate equation,

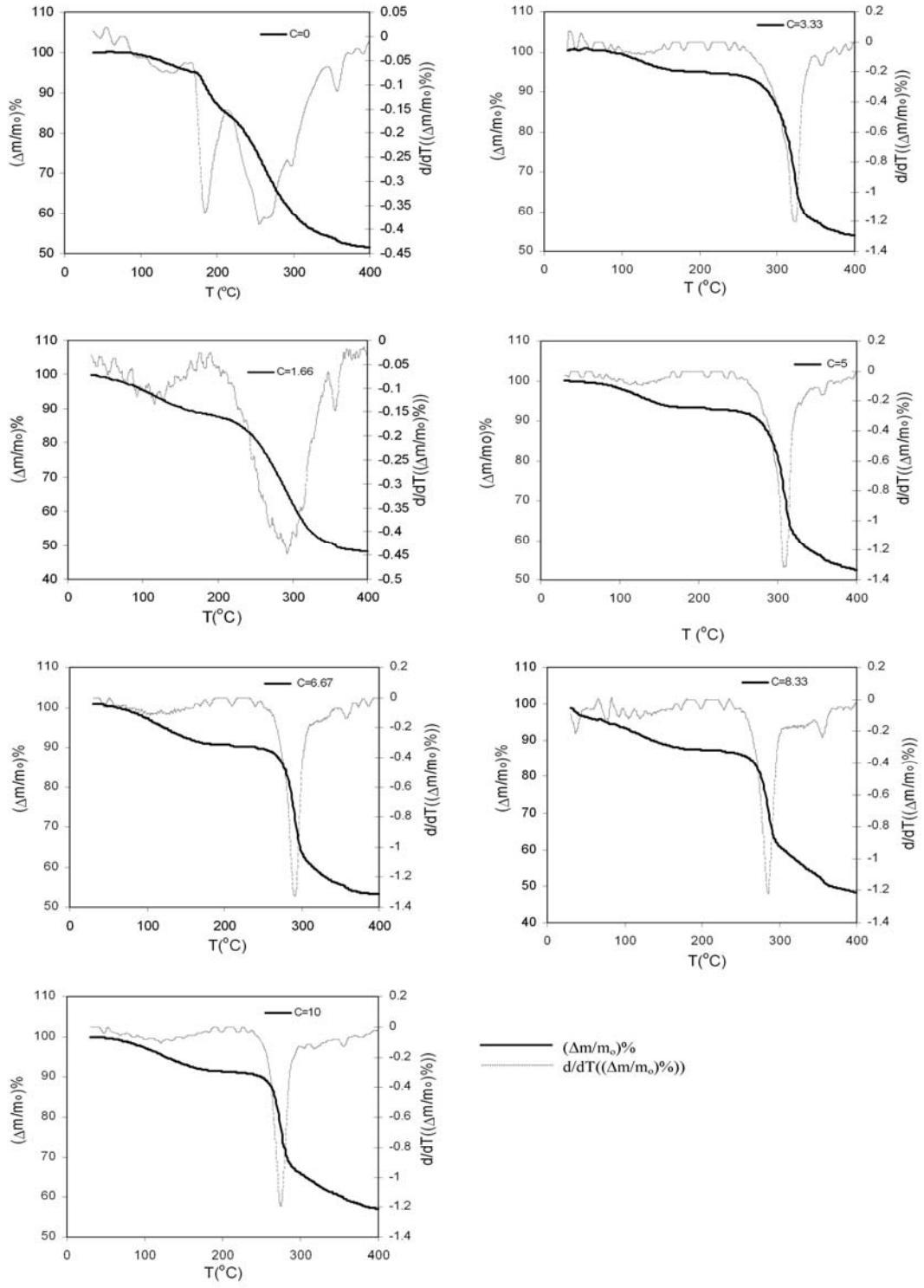

Fig.(4.4): TGA thermograms (weight loss fraction) versus temperature for (a) C=0, (b) C=1.66, (c) C=3.33, (d) C=5, (e) C= 6.67, (f) C=8.33 & (g) C=10 polymer electrolyte films.

Table (4.2): The Kinetic parameters of the thermal degradation from TGA curve.

C ($NaI/CuCl_2$)	$T_{onset(1)}$ (°C)	$T_{onset(2)}$ (°C)	$T_{Max\ loss}$ (°C)	Initial Mass (mg)	Area under curve (mg.°C)
0	92.4	233	257	2.41	693.5
1.66	58	240.5	294	3.38	979.7
3.33	93	267	323	2.61	840.4
5	80	267	310	3.1	973.2
6.67	65.5	276.5	291	2.38	722.7
8.33	-	270	286	2.19	637.8
10	66	262.5	275	3.67	1127.9

Table (4.3): The values of the apparent activation energy, E, of the prepared samples.

C ($NaI/CuCl_2$)	Activation energy (eV)
0	0.24
1.66	0.28
3.33	0.97
5	0.85
6.67	1.07
8.33	1.27
10	1.1

$$\frac{d\alpha}{dt} = k(1-\alpha)^n \qquad (4.2)$$

where $\alpha = \frac{w_i - w_t}{w_i - w_f}$, w_i is the initial weight, w_t is the weight at given temperature and w_f is the final weight of the sample, where k can be represented by Arrhenius equation,

$$k = Ae^{(-E/RT)} \qquad (4.3)$$

E is the activation energy of polymer decomposition, R is the universal gas constant, T is the absolute temperature and A is the frequency factor. According to Coats-Redfern [69] n is the reaction order. The decomposition kinetics of the present PVA electrolyte with different ratios of C can be expressed by the following relation,

$$\log[\frac{-\log(1-\alpha)}{T^2}] = \log[\frac{(1-2RT/E)AR}{\beta E}] - \frac{E}{2.303RT} \quad (n=1) \qquad (4.4)$$

where β is the heating rate. By plotting $\log[-\log(1-\alpha)/T^2]$ against $1000/T$ for each sample Fig.(4.5), straight lines are obtained. Then, the apparent activation energies for the decomposition are calculated and given in table (4.3). From this table, its clear that, values of the activation energy in general increases with increasing the salt concentration which indicate the improvement of polymer composite with increasing C ratio.

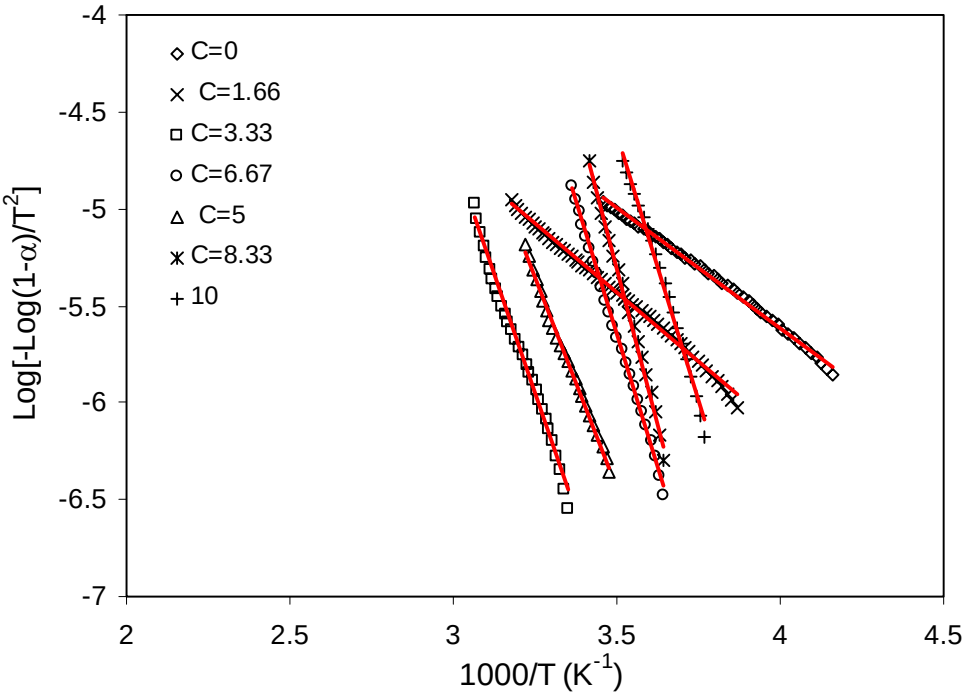

Fig.(4.5): The dependence of $\log[\frac{-\log(1-\alpha)}{T^2}]$ **on** $1000/T$ **for polymer electrolyte films.**

4.A.4 FTIR Spectroscopy

FTIR spectroscopy has been used to analyze the interactions among atoms or ions in PVA polymer electrolyte. These interactions can induce changes in the vibrational modes of the polymer electrolyte. The FTIR spectrum of pure PVA and PVA doped with the different ratio of C ($NaI/CuCl_2$) are shown in Fig.6(a–g). The FTIR spectrum exhibits several bands characteristic of stretching and bending vibrations of O–H, C–H, C=C and C–O groups.

The complete assignments for the frequencies of different groups and vibrational modes of PVA and PVA: C ($NaI/CuCl_2$) is presented in table (4.4). From the infrared spectra, it can be noticed that the variation of C ratio causes some observable changes in the spectrum of PVA. It induces some new absorption bands and slight changes in the intensities of some absorption bands. The new absorption bands may be correlated, likewise, to defects induced by the charge-transfer reaction between the polymer chain and the dopant.

From the spectra, The FTIR spectrum of pure PVA shows broad and strong bands are observed at 3459 cm^{-1} is assigned to O–H stretching vibration of hydroxyl groups of PVA. A weak band is observed at 2163 cm^{-1}, which has been assigned to the combination frequency of (CH + CC). The bands at 1673 cm^{-1} corresponds to an acetyl C=O group and can be explained on the basis of intra/inter molecular hydrogen bonding with the adjacent OH group. The strong band at 1118 cm^{-1} has been attributed to the stretching mode of CO groups [28].

In case of PVA electrolyte with different C ratio, FTIR spectra shows shift in some bands and change in the intensities of other bands comparing with pure PVA. This indicates the considerable interaction between the polymers and salt. The band observed at 2950 cm^{-1} (for C=8.33) indicates an asymmetry in stretching mode of CH_2 group [28]. The observed beak at 1736 cm^{-1} (for C=1.66)

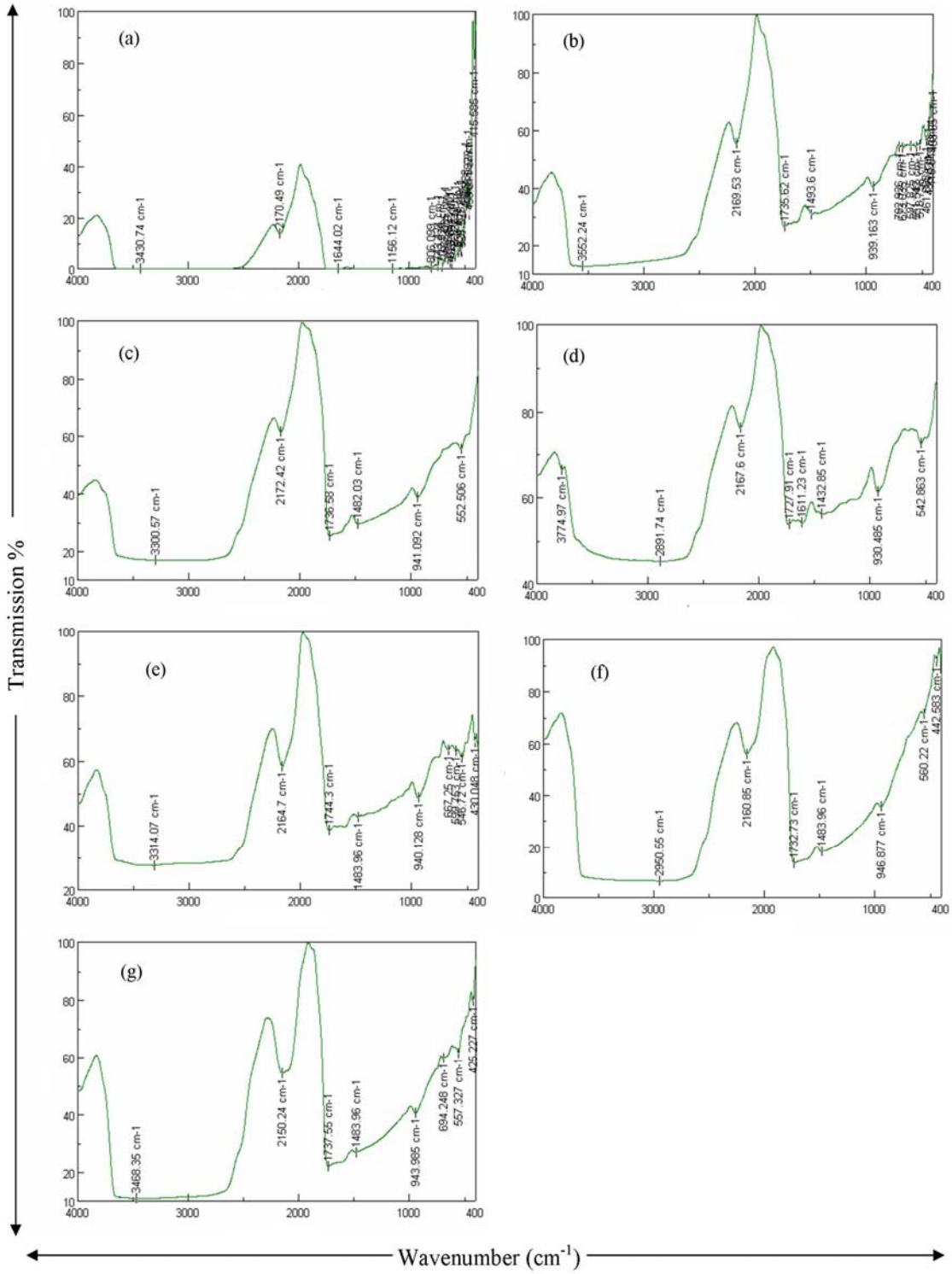

Fig.(4.6): FTIR spectra for polymer electrolyte films (a) C=0, (b) C=1.66, (c) C=3.33, (d) C=5, (e) C= 6.67, (f) C=8.33 & (g) C=10.

Table (4.4): FT-IR absorption bands positions and their assignments for pure PVA and PVA with different ratio of C ($NaI/CuCl_2$).

Vibration frequency (cm^{-1})	Band assignment	PVA:C ($NaI/CuCl_2$)						
		C=0	C=1.66	C=3.33	C=5	C=6.67	C=8.33	C=10
Pure PVA		3430	3552	3300	3774	3314	--	3468
3459	O–H stretching							
2950	CH_2 asymmetric stretching	--	--	--	--	--	2950	--
2859	CH_2 symmetric stretching	--	--	--	2891	--	--	--
2163	combination frequency of (CH + CC)	2170	2169	2172	2167	2164	2160	2150
1736	C=C stretching	--	1735	1736	1727	1744	1732	1737
1673	C=O stretching	1644	--	--	1611	--	--	--
1482	O–H and C–H bending of PVA	--	1493	1482	1432	1483	1483	1483
1118	CO stretching mode	1156	--	--	--	--	--	--
910	CC stretching mode	--	939	941	930	940	946	943

was assigned to C=C stretching and it is found to be shifted to lower wave numbers in the complexed system to the wave numbers 1735, 1727, 1744, 1732 and 1737 respectively [70]. The peak at 1482 cm^{-1} (for C=1.66) corresponds to O–H and C–H bending of PVA [71] and it is found to be shifted to 1493, 1432, 1483, 1483 and 1483 respectively.

These changes are attributed to the interaction between the salt with the host polymer matrix. This confirms the complex formation between PVA and the salt.

Section (B)

Electrical and Dielectric Properties of PVA/Cui Polymer Electrolytes

4.B.1 Complex Impedance Analysis

Complex impedance spectroscopy (CIS) is an important technique in view of its simplicity and clarity in describing the electrical processes occurring in a system on applying an ac signal as input perturbation. The output response, when plotted in a complex plane plot, appears in the form of a succession of semicircles representing electrical phenomena due to bulk material, grain boundary effect and interfacial phenomena if any. The complex impedance analysis method was used to determine the bulk electrical conductivity σ_b and relaxation time τ of all samples. The impedance was analyzed to a real part Z' and imaginary part Z'' on the complex plane at temperature range 303–373K. Fig.(4.7) illustrates the impedance plot of the imaginary part Z'' against the real part Z' for polymer electrolytes at two different temperature (T=303 & 313K). The impedance plot, in general, shows an arc (semicircle) its centre below the Z' axis where the semicircle reflects the impedance of charge transfer. The intersection with Z' axis represents the sample bulk resistance, R_b. It is also clear that the circle diameter decreases with increasing salt concentration and temperature. The values of bulk conductivity σ_b of the polymer electrolytes were obtained ($\sigma_b = d / R_b A$, where d is the film thickness and A is its effective area) for different ratios of C in the polymer electrolyte films. The values of σ_b increase exponentially with increasing C ratio according to the relation [72],

$$\sigma_b = \sigma_{bo} \exp(C / C_o) \qquad (4.5)$$

where σ_{bo} is the bulk conductivity for pure PVA and C_o is the effective NaI/$CuCl_2$ ratio (the onset of salt conductivity enhancement).

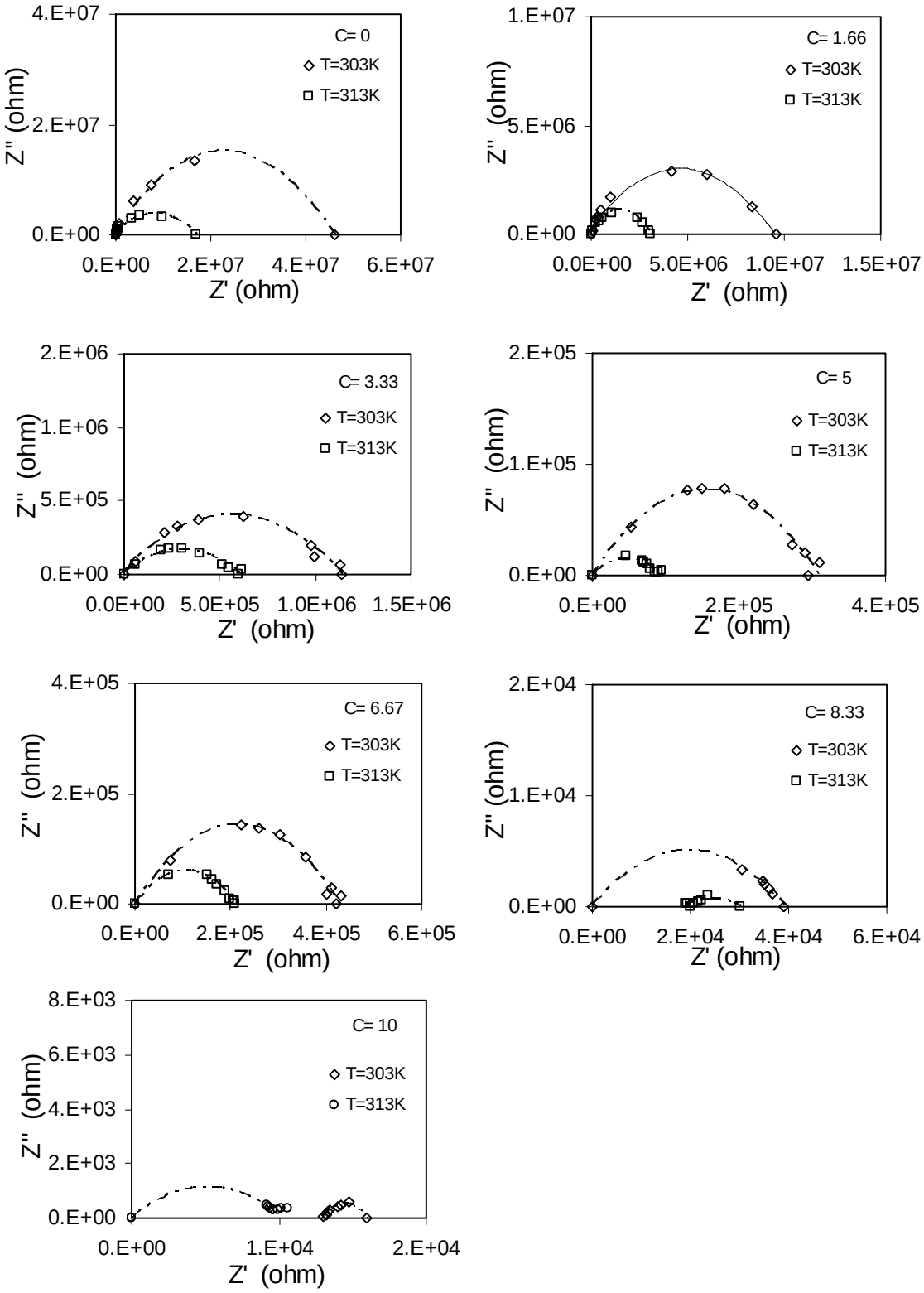

Fig.(4.7): Complex Cole-Cole plot of impedance for polymer electrolyte films at T=303K & T=313K.

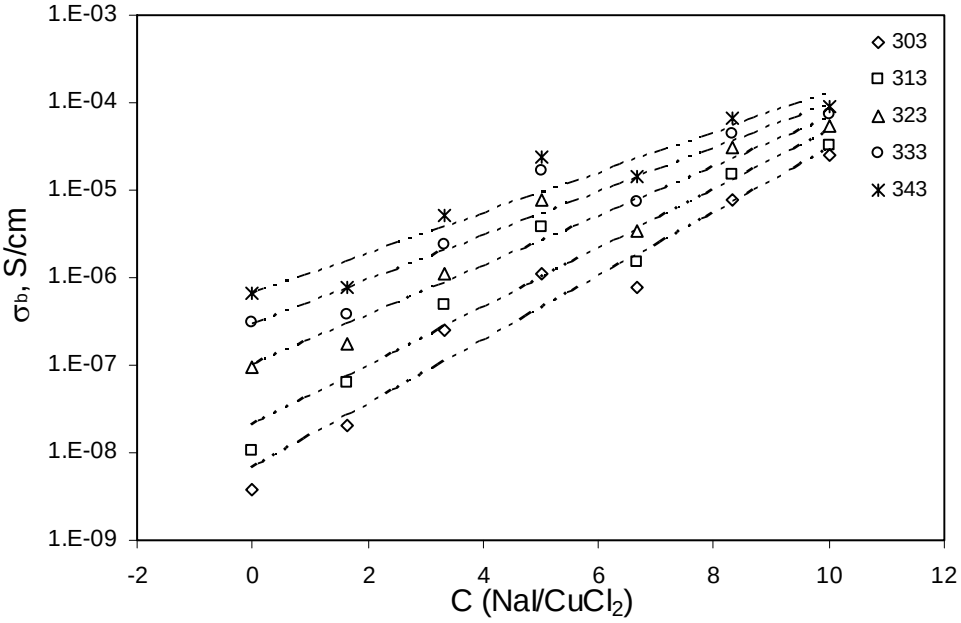

Fig.(4.8): Bulk conductivity σ_b against C ($NaI/CuCl_2$) ratio at different temperatures for polymer electrolyte films.

Fig.(4.8) shows the relation between σ_b and C ratio. The values of σ_{bo} and C_o are obtained by least square fitting of equation (4.5) at different temperature and are summarized in table (4.5). The conductivity of the present polymer electrolyte can be explained as, at low concentration of CuI, the conductivity is mainly due to the host polymer matrix. As the concentration of CuI phase increases beyond C_o, the conductivity is due to hole conduction in CuI crystallites besides oxidation/reduction of iodine in polymer matrix. In other words as the C ratio increases, an excess of NaI dissolved in the polymer matrix contributes with the positive holes of CuI particles in conduction process. The increase in the conductivity with increasing salt concentration can be related to the increase in the number of mobile charge in the polymer electrolyte which can be described by the relation [73],

$$\sigma = n \times q \times \mu \qquad (4.6)$$

where n, q and μ representing the charge carrier concentration, charge of mobile carrier and the mobility, respectively.

The values of σ_b have been obtained at different temperature, Fig.(4.9) shows the variation of the bulk conductivity σ_b with temperature and it was found to obey the Arrhenius relation,

$$\sigma_b T = G \exp(-\frac{\Delta E_b}{kT}) \qquad (4.7)$$

where G is temperature pre-exponential factor, ΔE_b is the bulk activation energy. The values of the activation energy ΔE_b are obtained using the least square fitting of equation (4.7) and listed in table (4.6). It is clearly observed that ΔE_b decreases, where the value of bulk conductivity increases, with increasing C ratio.

Table (4.5): The deduced values of σ_{bo} and C_o for polymer electrolyte at different temperature.

T (K)	σ_{bo}	C_o
303	7×10^{-9}	1.19
313	2×10^{-8}	1.29
323	1×10^{-7}	1.54
333	3×10^{-7}	1.72
343	6×10^{-7}	1.88

Table (4.6): Obtained values of the activation energy of the Bulk conductivity for polymer electrolyte films.

C (NaI / $CuCl_2$)	ΔE_b, (eV)
0	1.24
1.66	0.83
3.33	0.69
5	0.7
6.67	0.69
8.33	0.5
10	0.33

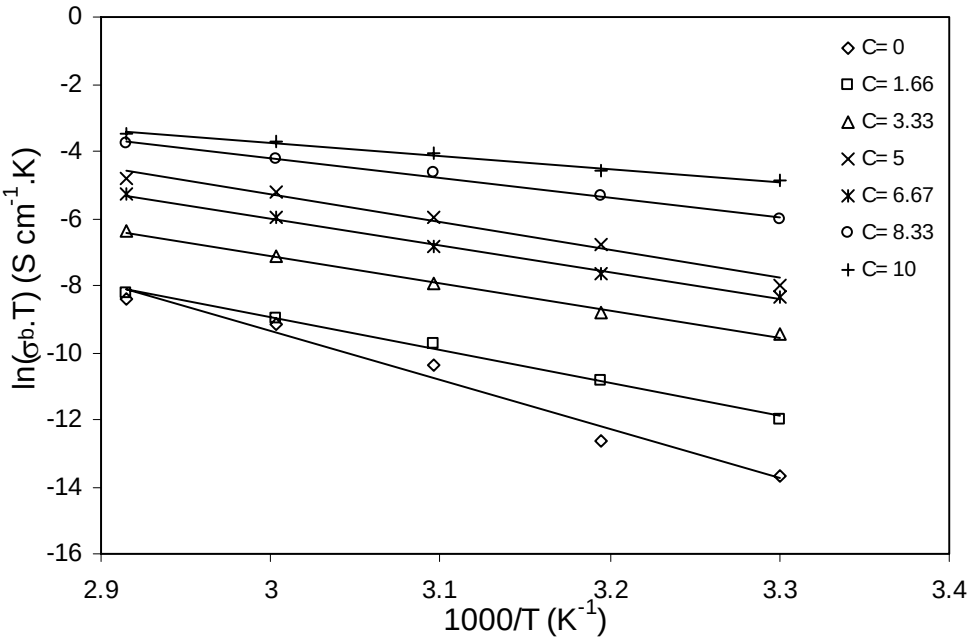

Fig.(4.9): Temperature dependence of bulk conductivity σ_b for polymer electrolyte films.

4.B.2 AC Conductivity for PVA/CuI Polymer Electrolyte

4.B.2.1 Frequency Dependence of the Total Conductivity

Fig.(4.10) shows the variation of the total electrical conductivity $\sigma_{tot}(\omega)$ with the applied frequency, in the frequency range 100Hz to 100 KHz, for all samples at different temperature. It's evident that the frequency independent conductivity appears at low frequency range, which representing σ_{dc} (extrapolation of $\sigma_{tot}(\omega)$ at ω=0). The frequency dependence conductivity appears at high frequency, where the general behavior of $\sigma_{tot}(\omega)$ is increasing with frequency obeying a power law, $\sigma_{ac} = A\omega^{S}$. Therefore, the frequency dependence of the total conductivity can be expressed by the universal power law (UPL) [74]:

$$\sigma_{tot}(\omega) = \sigma_{dc} + \sigma_{ac} = \sigma_{dc} + A\omega^{S} \qquad (4.8)$$

where σ_{dc} is a frequency independent term representing the dc component, A is the frequency independent factor and s the frequency exponent.

The values of the exponent S are deduced at different temperatures for all samples using the least square fitting of equation (4.8) and represented in Fig.(4.11). It is noticed that the values of the power ($0 < S < 1$) decrease with increasing temperatures, indicating that the conduction mechanism can be understood on the basis of the correlated barrier hopping model (CBH) [75]. The exponent S increases towards to unity as T tends to the absolute Zero according to the relation [76]:

$$S = 1 - [\frac{6k_B T}{W_M}] \qquad (4.9)$$

(a)

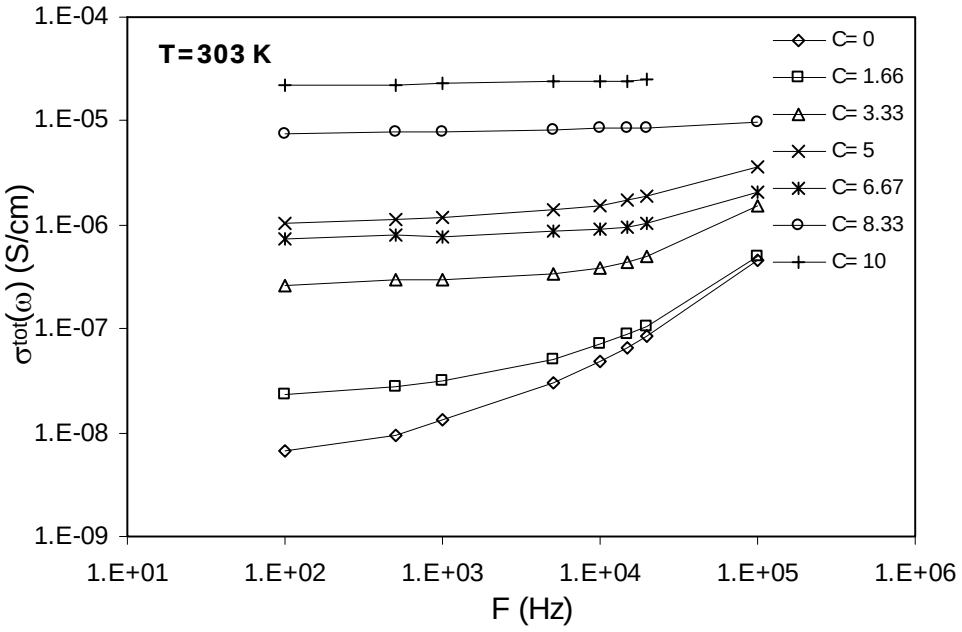

(b)

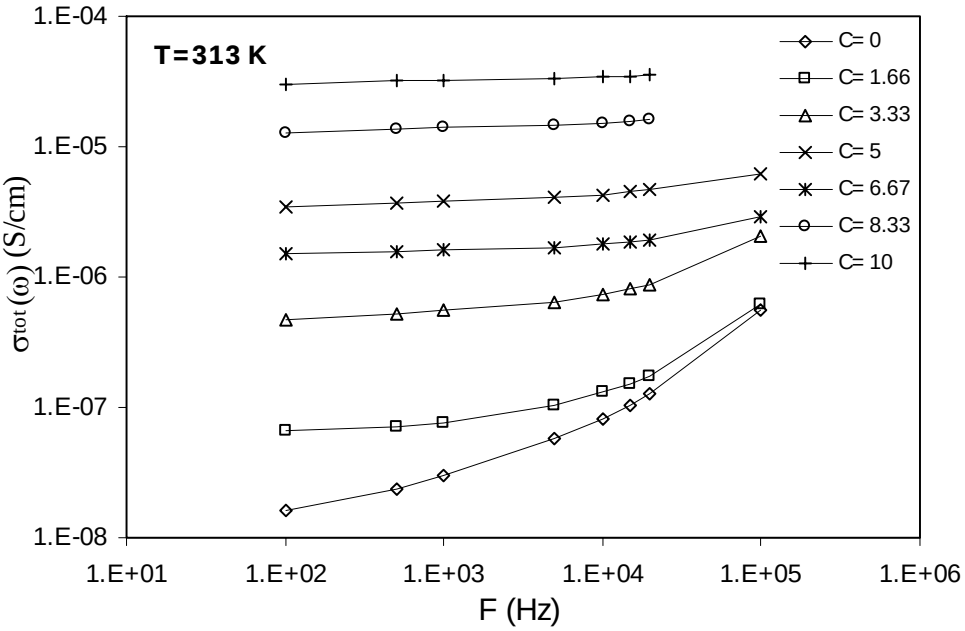

Fig.(4.10): Frequency dependence of the total conductivity $\sigma_{tot}(\omega)$ for polymer electrolyte films at different temperature.

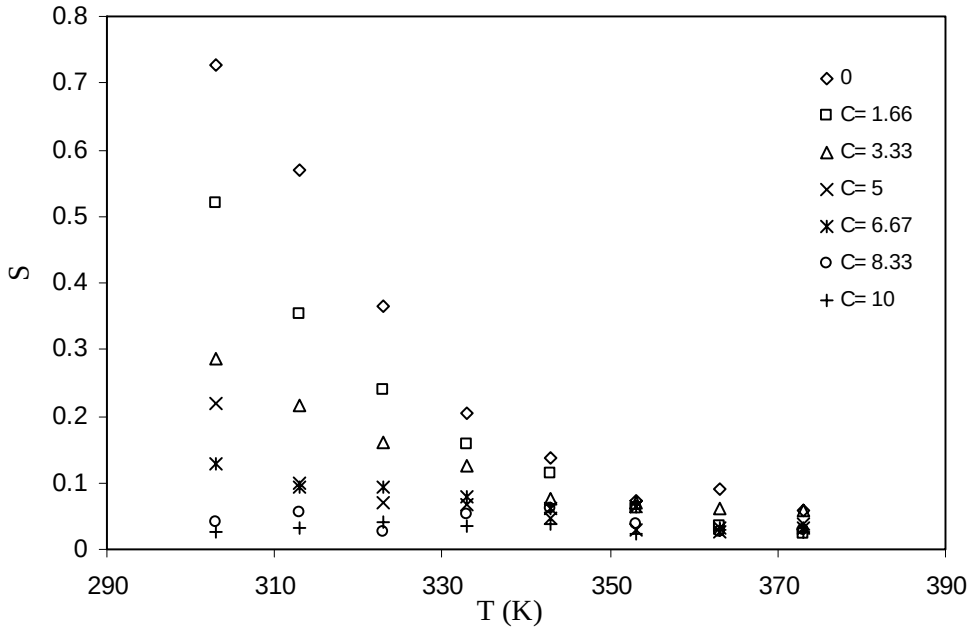

Fig.(4.11): Temperature dependence of the power S for polymer electrolytes at different C ($NaI/Cucl_2$) ratio.

where W_M is the activation energy of a single electron transport between degenerate sites.

In addition the transition between the nearly frequency independent region (dc conductivity) at low frequencies and that at intermediate frequencies (polarizing conductivity) may occur at a certain frequency ω_p (defined as the hopping frequency). In the high frequency region, the power law feature $\sigma(\omega)\alpha\omega^s$ is observed and conductivity sharply increases with frequency. The transition from the slow rise in conductivity to its abrupt increase in conductivity signifies the onset of conductivity relaxation. The UPL behavior observed in the sample agrees well with the prediction of the jump relaxation model. At low frequencies, ions travel much slower and so are able to jump from one site to another vacant site which contributes to the dc conductivity when the frequency is lower than ω_p. When frequency exceeds ω_p, $\sigma(\omega)$ increases proportionally with ω^S, where $S \prec 1$. This dispersion indicates that on time scales shorter than $1/\omega_p$, the ionic diffusion is non-random, that is the ions perform correlated forward–backward motions. The values of ω_p are obtained by assuming that the ac conductivity is nearly equal to dc conductivity at $\omega = \omega_p$ [77]:

$$\omega_p = \left(\frac{\sigma_{dc}}{A}\right)^{\frac{1}{S}} \qquad (4.10)$$

The obtained values of ω_p are listed in table (4.7).

Table (4.7): Values of the hopping rate ω_p at different temperature for polymer electrolyte films.

T K	ω_p , for different samples						
	C= 0	C= 1.66	C= 3.33	C= 5	C= 6.67	C= 8.33	C= 10
303	2.6×10^3	7×10^3	1.3×10^4	3.6×10^4	5.1×10^4	1.1×10^5	---
313	$3.\times10^3$	7.4×10^3	9.2×10^3	6.7×10^4	4.1×10^5	---	4.4×10^5
323	6.8×10^3	1.5×10^4	1.8×10^3	3.2×10^3	1.1×10^5	---	4.1×10^4
333	6.7×10^3	1.2×10^4	1.6×10^3	---	5.7×10^3	5.2×10^5	1.1×10^4

4.B.2.2 Temperature Dependence of the Total Conductivity

The temperature dependence of the total electrical conductivity $\sigma_{tot}(\omega)$ of all polymer electrolyte films at different fixed frequencies shown in Fig.(4.12). The plot shows that as the temperature increases the conductivity, in general, increases obeying Arrhenius relation,

$$\sigma_{tot}(\omega).T = C\exp(-\frac{\Delta E_{ac}}{kT}) \qquad (4.11)$$

where C is the pre-exponential factor, ΔE_{ac} is the ac activation energy, K is the Boltzmann constant and T is absolute temperature. The values of the activation energy ΔE_{ac} were obtained at different frequencies using the least square fitting for equation (4.11) and listed in table (4.8). It is observed that the decrease of the activation energy with increasing C ratio could be attributed to the increase in free iodine I_2 inside the polymer matrix and also production of P-type CuI, the increase of hole concentration. In addition the conductivity values of all polymer electrolytes under investigation do not show any abrupt change with temperature, indicating that there is no phase transition in the structure within the measured temperature range.

Druger et al. [78] have attributed the increase in conductivity with temperature in solid polymer electrolyte to segmental (i.e. polymer chain) motion, which results in an increase in the free volume of the system. This, in turns, results in the ions to hop from one site and provides a pathway for ions to move. In other words, the segmental movement of the polymer facilitates the translational ionic motion. From this, it is clear that the ionic motion is due to translational motion/hopping facilitated by the dynamic segmental motion of the polymer, the increase of charge carrier mobility. As the amorphous region increases the polymer chain acquires faster internal modes in which bond

rotations produce segmental motion to favor inter and intra-chain ion hopping, and thus the degree of conductivity becomes high [79].

(a)

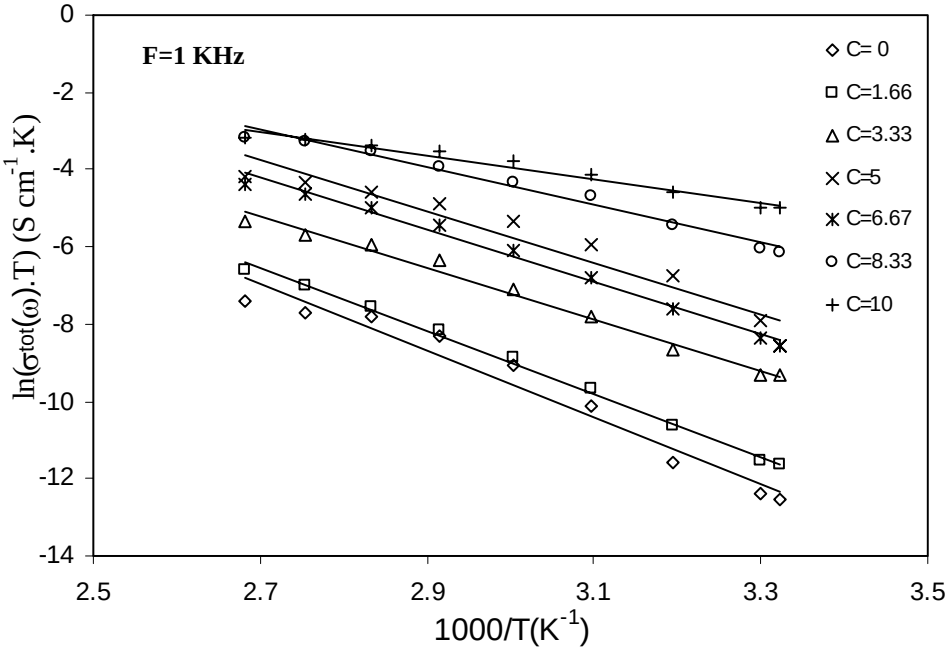

(b)

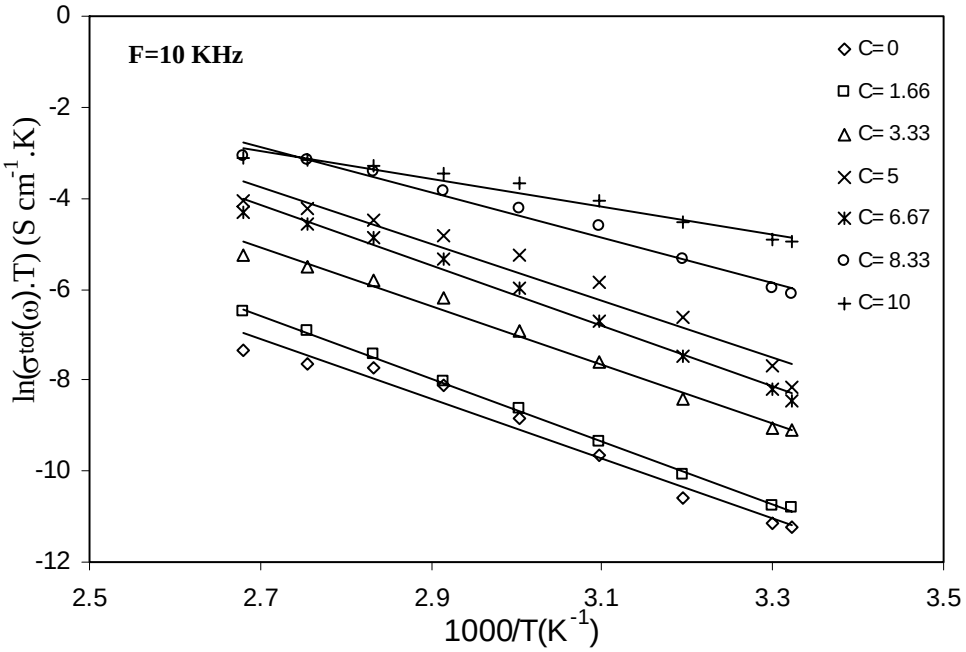

Fig (4.12): Temperature dependence of the total conductivity $\sigma_{tot}(\omega)$ for polymer electrolyte films at different frequencies.

Table (4.8): Extracted values of the activation energy of the ac conductivity at different frequencies for polymer electrolyte films.

C ($NaI/CuCl_2$)	ΔE_{ac}, eV		
	1 KHz	5 KHz	10 KHz
0	0.74	0.62	0.56
1.66	0.69	0.63	0.59
3.33	0.56	0.56	0.54
5	0.56	0.55	0.53
6.67	0.58	0.57	0.57
8.33	0.41	0.42	0.42
10	0.26	0.26	0.26

4.B.3 Dielectric Properties of PVA/CuI Polymer Electrolytes

4.B.3.1 Frequency Dependence of the Dielectric Parameters

Fig.(4.13) show the variation of the dielectric constant ε' versus frequency at temperature 303 and 313K, respectively. It can be noticed that ε' decreases monotonically with increasing frequency in the frequency range of $\omega\tau >> 1$ for all polymer electrolyte films. This behavior can be described by the Debye dispersion relations [80],

$$\varepsilon' \cong \varepsilon_\infty + \frac{\varepsilon_s - \varepsilon_\infty}{1 + \omega^2 \tau^2} \qquad (4.12)$$

The increase in the dielectric constant represents a fractional increase in charges within the polymer electrolyte. The dependence of charge carrier concentration n upon the dissociation energy U and dielectric constant ε' can be explained by the equation [81],

$$n = n_o \exp(-U / \varepsilon' kT) \qquad (4.13)$$

where k is the Boltzmann constant and T the absolute temperature.

Upon addition of C ratio in the electrolyte the dielectric constant ε' has been experimentally found to increase. The increase in the value of dielectric constant indicates that there is an increase in charge carrier concentration and hence the increase in conductivity [82]. The decrease in the dielectric constant for further addition of C ratio, leads to the formation of ion aggregation, which causes a fall in mobility of charge carriers and cause a significant fall in ionic conductivity in accordance with equation (4.6).

The variation of dielectric constant ε' as a function of frequency for all polymer electrolytes at different temperatures (Fig.(4.13)) indicates that at low

(a)

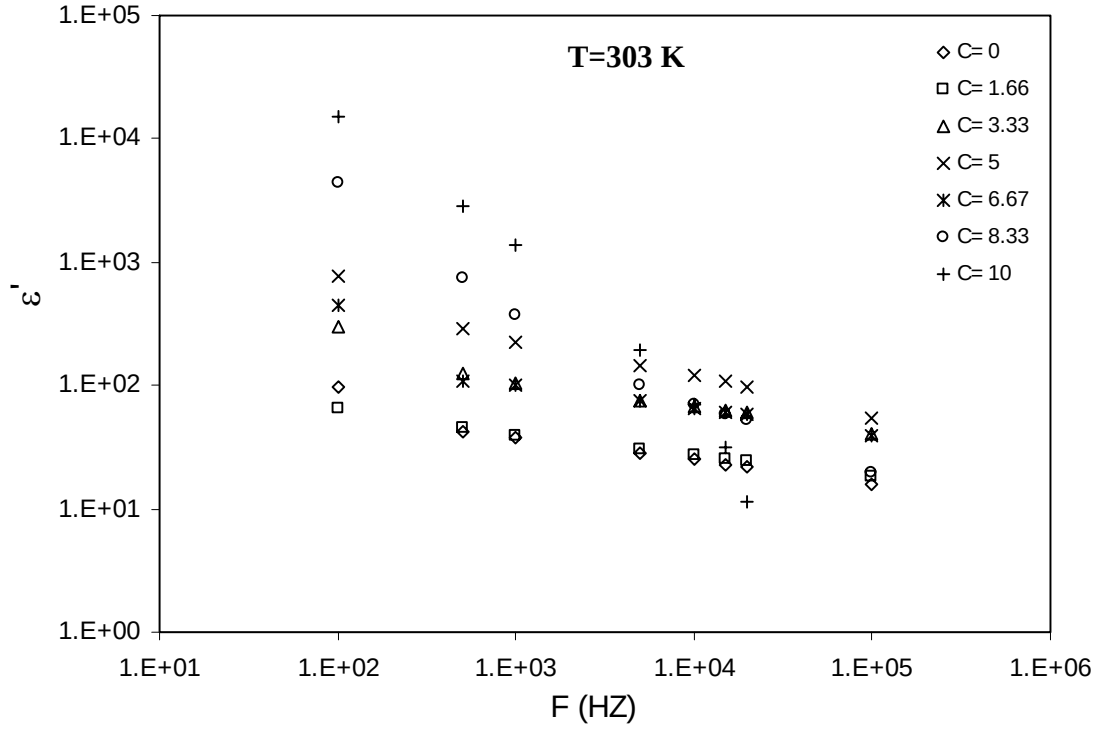

(b)

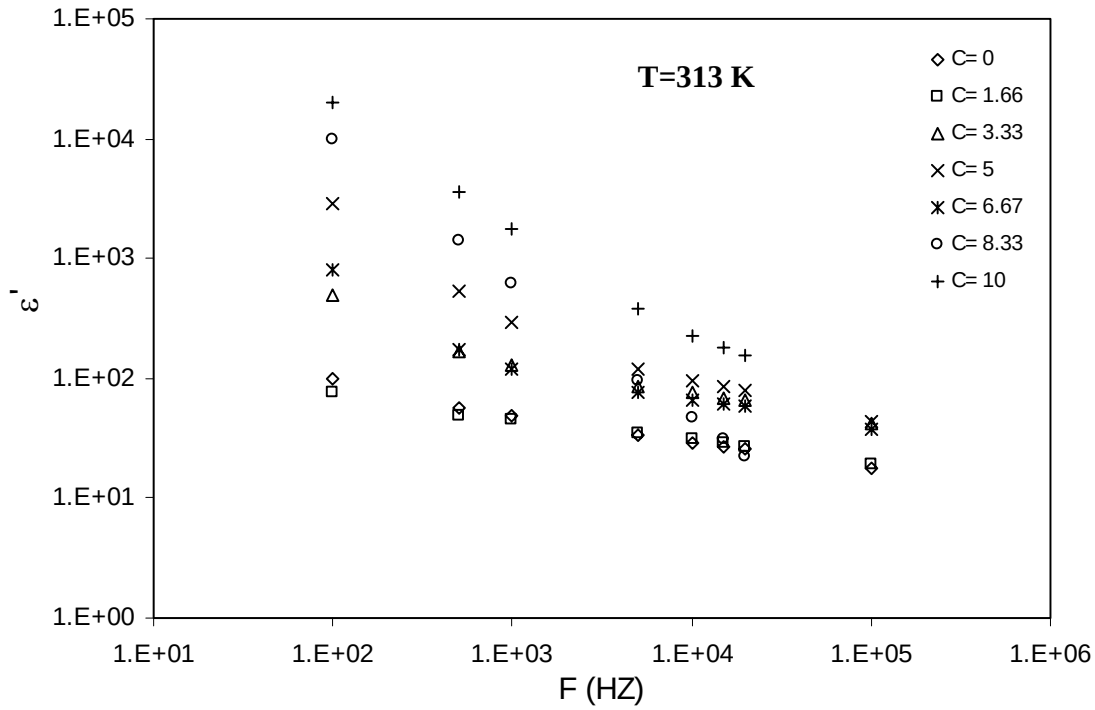

Fig.(4.13): Frequency dependence of dielectric constant ε' for polymer electrolyte films of different C ratio.

frequencies the dielectric constant is high due to the accumulation of the charge carriers near the electrodes. There is a decrease in dielectric constant towards higher frequencies due to the high periodic reversal of the applied field, the polarization due to the charge accumulation decreases that lead to the decrease in the value of dielectric constant.

Fig.(4.14) shows the variation of the dielectric loss ε'' versus frequency, 100Hz to 100KHz, at temperature 303 and 313K. It can be noticed that ε'' decrease monotonically with increasing frequency in the frequency range of $\omega\tau >> 1$ for all polymer electrolyte films. This behavior can be described by the Debye dispersion relations [80],

$$\varepsilon'' \equiv \frac{(\varepsilon_s - \varepsilon_\infty)\omega\tau}{1+\omega^2\tau^2} \qquad (4.14)$$

Curves in Fig.(4.14) reveal that the values of ε'' sharply raise at low frequency. This indicates that electrode polarization and space charge effects have occurred confirming the non-Debye dependence [83]. While ε'' decreased with increasing frequency until to be relatively constant at higher frequencies. This is because, at higher frequencies periodic reversal of the field takes place so rapidly that the charge carriers will hardly able to orient themselves in the field direction resulting in the observed decrease of dielectric constant and dielectric loss.

(a)

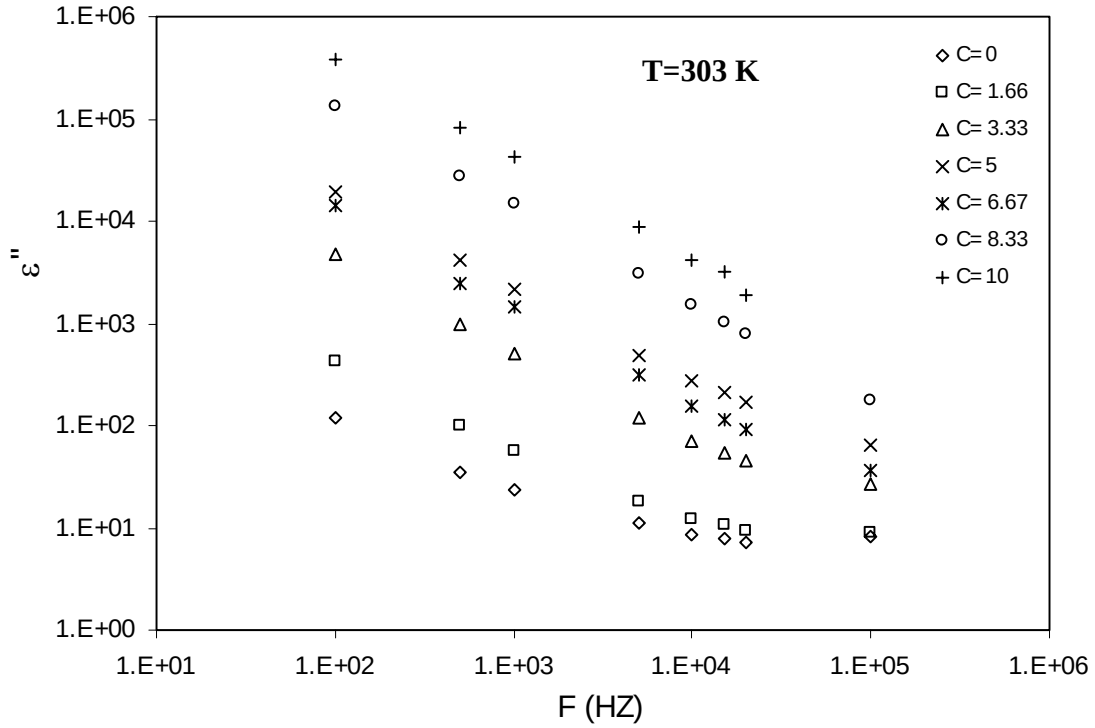

(b)

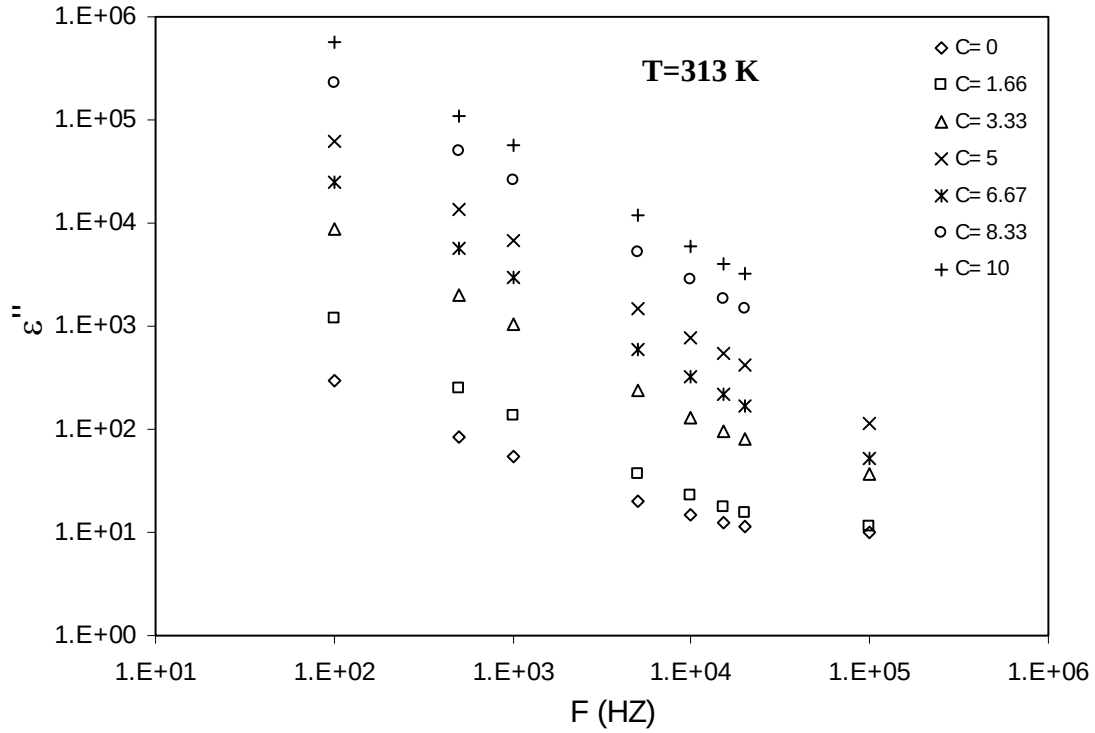

Fig (4.14): Frequency dependence of dielectric loss ε'' for polymer electrolyte films of different C ratio.

4.B.3.2 Temperature Dependence of the Dielectric Parameters

Fig.(4.15) shows the variation of the dielectric constant ε' versus temperature (T), at two constant frequencies 1KHz and 5KHz, respectively. It is clear that ε' increases with increase temperature. The variation of ε' with temperature is different for non-polar and polar polymers. In general, non-polar polymers ε' is independent of temperature. But in the case of polar polymers the ε' increases with the increase of temperature. This behavior is typical of polar dielectrics, in which the orientation of dipoles is facilitated with the rising temperature and thereby the permittivity is increased [84]. The dielectric constant increases with temperature because the orientation is facilitated as the temperature increases. The increasing value of ε' with increasing temperature is mainly due to the migration polarization of the mobile ions.

Fig.(4.16) show the variation of the dielectric loss ε'' versus temperature (T), at two constant frequencies 1KHz and 5KHz, respectively. It is clear that ε'' increases with increase temperature. The relationship between the conductivity and the dielectric loss factor can be given by [73],

$$\varepsilon'' = \frac{\sigma}{\omega \varepsilon_o} \qquad (4.15)$$

Since σ is dependent on temperature, the dielectric loss is strongly dependent on temperature and hence the increase in ε'' value with increase of temperature.

(a)

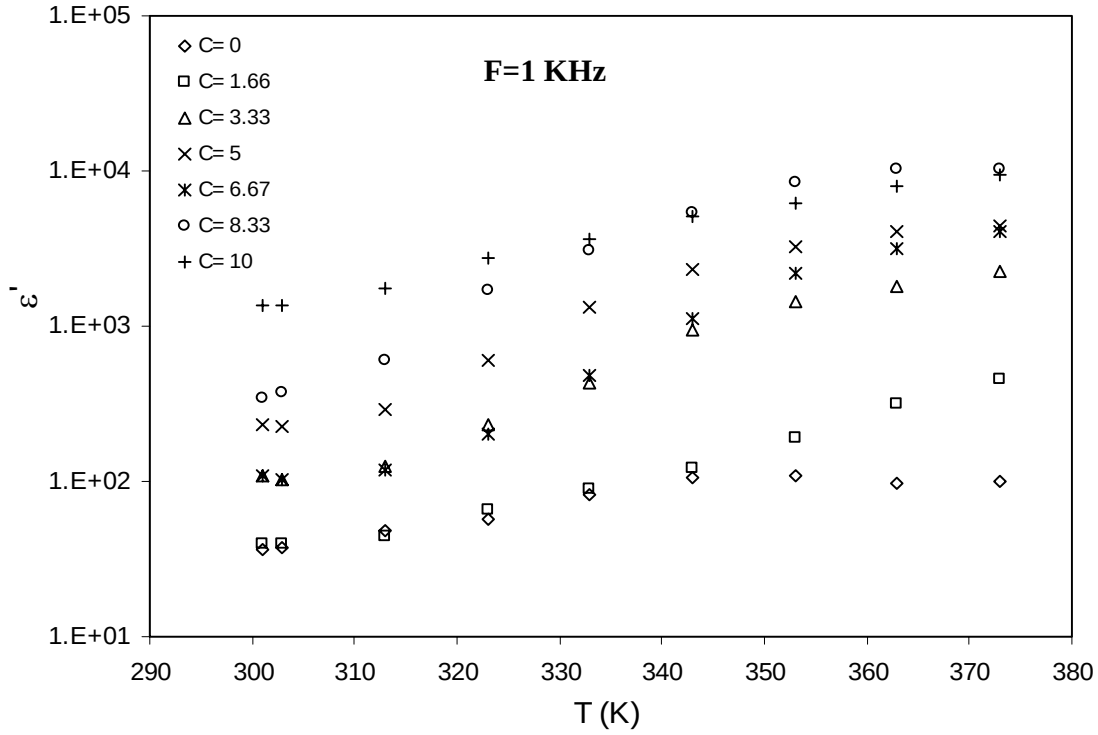

(b)

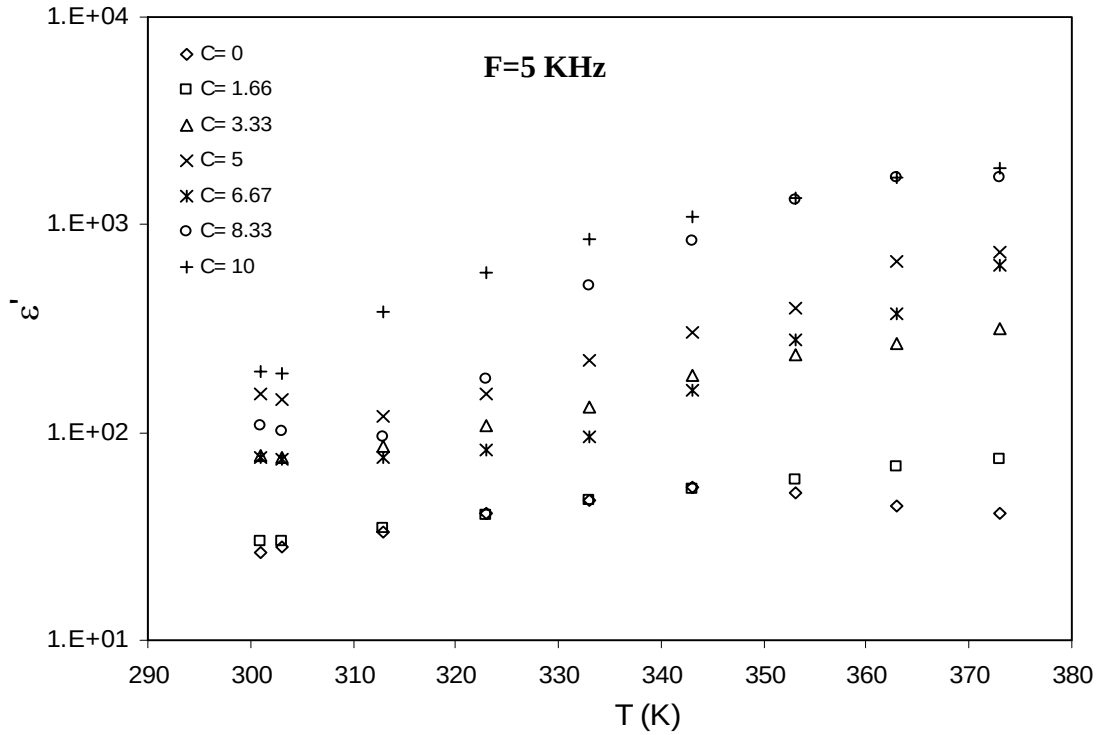

Fig (4.15): Temperature dependence of dielectric constant ε' for polymer electrolyte films of different C ratio.

(a)

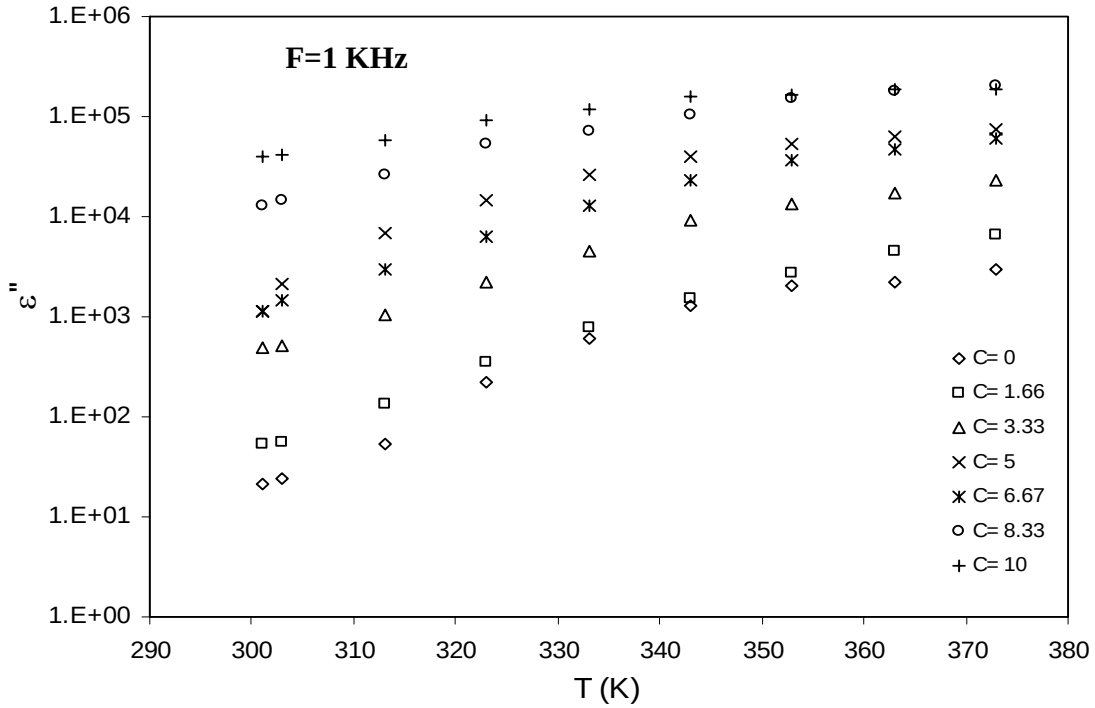

(b)

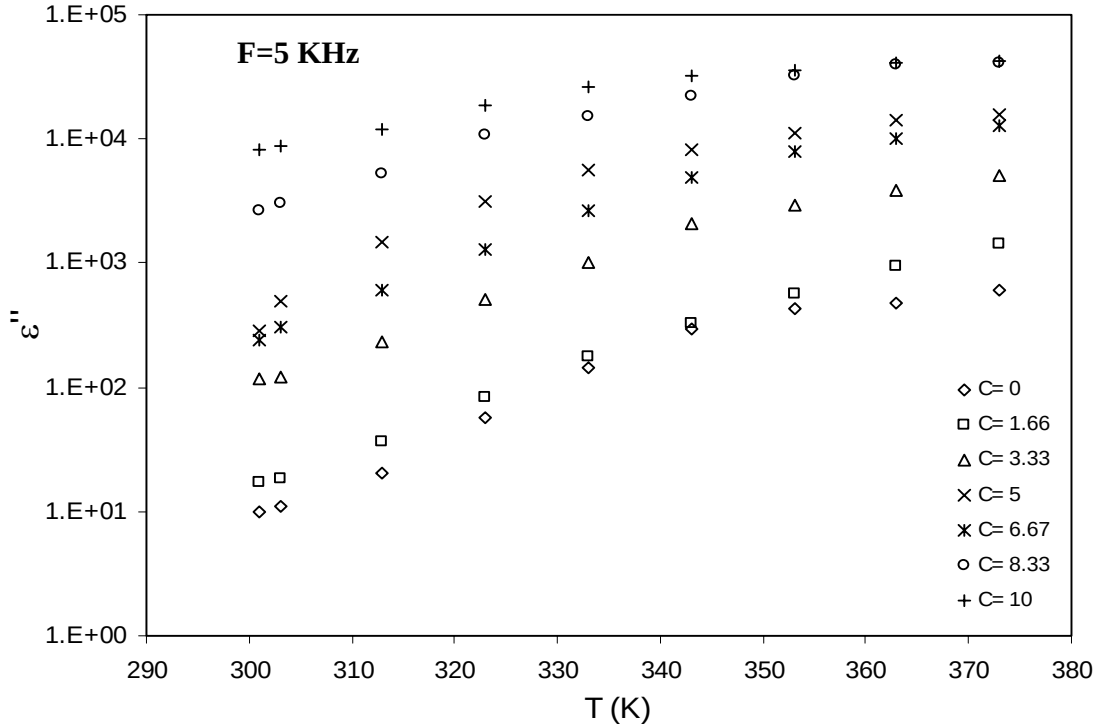

Fig.(4.16): Temperature dependence of dielectric loss ε'' for polymer electrolyte films of different C ratio.

From the Cole-Cole analysis the relaxation time τ has been obtained at different temperatures for all compounds using the following equation [59],

$$\frac{V}{u} = (\omega\tau)^{1-h} \qquad (4.16)$$

where V and u are the two sides of the triangle intersected at the semicircle and $h = 2\pi/\alpha$ where α is the angle of the diameter to Z'-axis as shown in Fig.(4.17).

The obtained values of the relaxation time for all polymer electrolyte films at different temperature were calculated using equation (4.16) and summarized in table (4.9). It can be noticed that the values of the relaxation time decrease with increasing ratio C and also with increasing temperature.

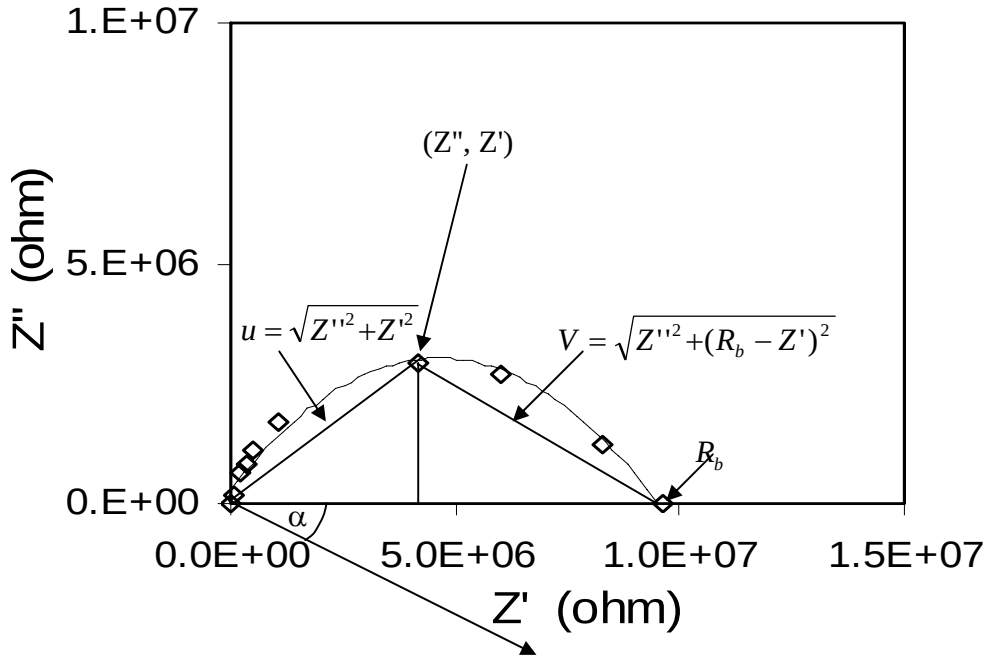

Fig.(4.17): The Cole-Cole diagram to obtain dipole relaxation time.

Table (4.9): Obtained values of relaxation time τ at different temperatures for polymer electrolyte films.

C (NaI/$CuCl_2$)/T(K)	303	313	323	333	343
0	2.69×10^{-3}	7.36×10^{-4}	4.84×10^{-5}	1.2×10^{-5}	5.75×10^{-6}
1.66	2.03×10^{-4}	5.95×10^{-5}	2.02×10^{-5}	9.06×10^{-6}	4.39×10^{-6}
3.33	2.69×10^{-5}	1.55×10^{-5}	7.08×10^{-6}	2.08×10^{-6}	8.61×10^{-7}
5	1.02×10^{-5}	1.48×10^{-6}	5.54×10^{-7}	-	-
6.67	7.24×10^{-6}	3.28×10^{-6}	1.1×10^{-6}	2.96×10^{-7}	-
8.33	4.04×10^{-7}	-	-	-	-
10	-	6.04×10^{-7}	1.6×10^{-7}	1.23×10^{-7}	8.99×10^{-8}

Section (C)

Optical Absorption of PVA/CuI Polymer Electrolytes

4.C.1 Ultraviolet and Visible Analysis

The absorption spectra for nanocomposite polymer electrolyte films were recorded in the wavelength range (190-1100 nm) and are shown in Fig.(4.18). The observed spectra are characterized by the main absorption edge for all curves that shifted towards higher wavelength with increasing filler content. For C=0 the absorption started at wavelength 400nm, while for different ratios of C the absorption is observed at higher wavelength 600nm. These indicate the complexation between the filler and the blends and may also be due to change in crystallinity due to adding the filler [85]. Fig.(4.18) shows a shift in both absorption bands and band edges towards the higher wavelengths with different absorption intensity for the doped PVA. These shifts in the bands indicate the formation of inter/intra molecular hydrogen bonding mainly between CuI and iodine ions with the adjacent OH groups. As the salt concentration increases, inter/intra hydrogen bonding increases and hence absorption. This is in accordance with the Beer's law [86], i.e. the absorption is proportional to the number of absorbing molecules. The shift in absorption edge in the doped PVA reflects the variation in the energy band gap, which arises due to the variation in crystal structure of the polymer matrix.

4.C.2 Determination of Optical Energy Gap (E_g)

The study of optical absorption gives information about the band structure of organic compound. Semiconductors are generally classified into two types: (i) direct band gap and (ii) indirect band gap. In direct band gap, the top of the valence band and the bottom of conduction band both lie at the same zero crystal momentum (wave vector). If the bottom of conduction band does not

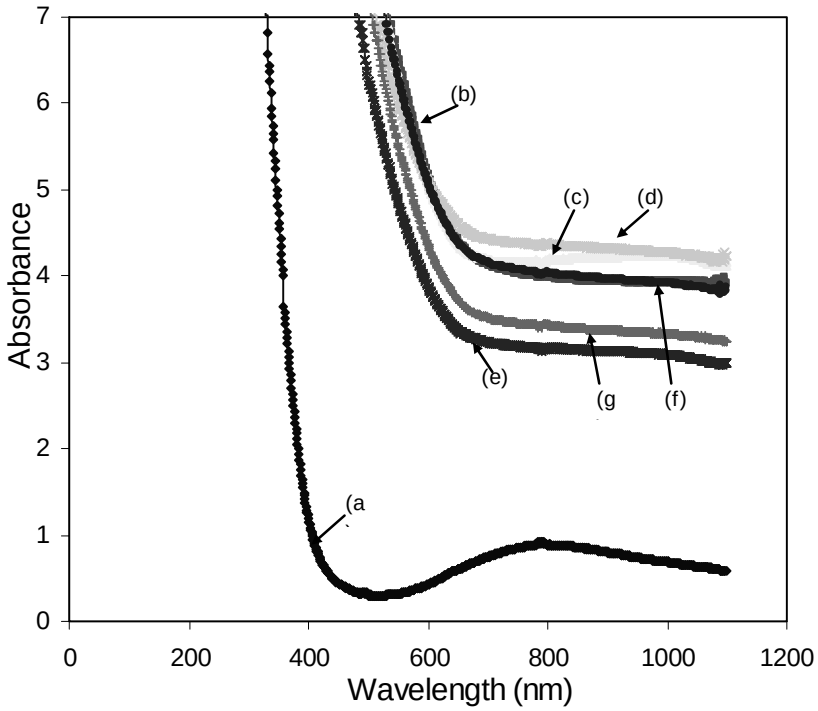

Fig.(4.18): UV-Vis optical absorption versus wavelength for polymer electrolyte films (a) C=0, (b) C=1.66 (c) C=3.33, (d) C=5, (e) C= 6.67, (f) C=8.33 & (g) C=10.

correspond to zero crystal momentum, then it is called indirect band gap. In indirect band gap materials transition from valence to conduction band should always be associated with a phonon of the right magnitude of crystal momentum [87]. Davis and Shalliday [88] reported that near the fundamental band edge, both direct and indirect transitions occur and can be observed by plotting $(\alpha h\upsilon)^{1/n}$ as a function of photon energy ($h\upsilon$). Concerning the optical transitions resulting from photons of energy $h\upsilon \succ E_g$, the present optical data can be investigated according to the following relation ship for the near edge optical absorption [56],

$$\alpha(\upsilon)h\upsilon = A(h\upsilon - E_g)^n \qquad (4.17)$$

where α is the absorption coefficient, υ is the frequency, h is the Planck's constant, A is a constant, E_g is the optical energy band gap between the valence and the conduction bands and n is the power that characterizes the transition process. The absorption coefficient (α) can be determined as a function of frequency using the formula [89]:

$$\alpha = 2.303 \times \frac{A}{d} \qquad (4.18)$$

where A is the absorbance and d is the thickness of the sample under investigation.

The direct optical band gaps were obtained from the linear plots of $(\alpha h\upsilon)^2$ versus $h\upsilon$ as shown in Fig.(4.19) for all sample. The extrapolations of the lines of $(\alpha h\upsilon)^2$ versus $h\upsilon$ for which $(\alpha h\upsilon)^2$ = 0, give the direct optical band gap E_{gd} and it was listed in table (4.9).From the table we find that the increase of C ratio has been small significant change on the optical gap width which mainly depends on the CuI particle size in the polymer matrix. As the size of semiconductor particles decreases to the nanoscale, the band gap of the

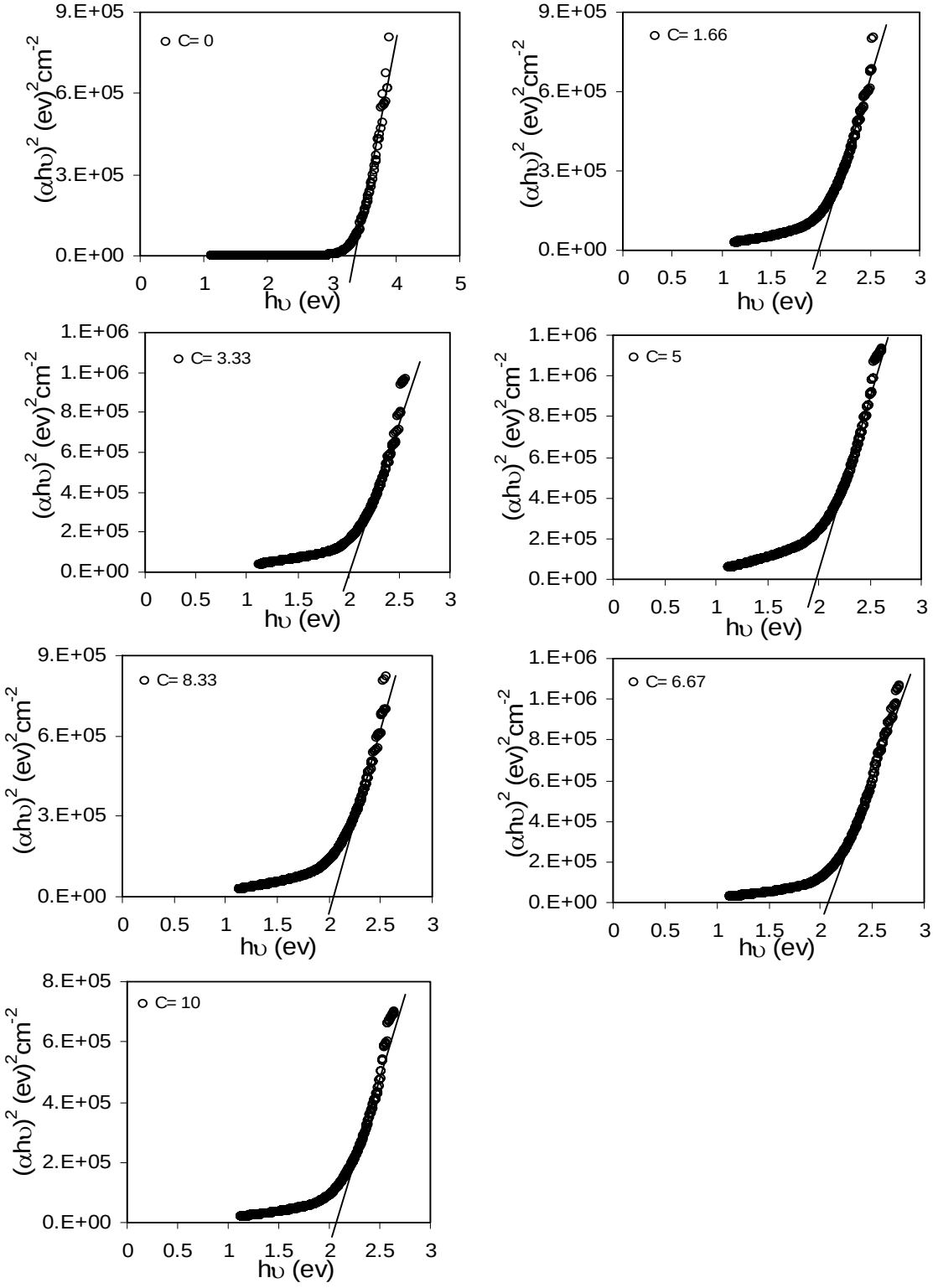

Fig.(4.19): The dependence of $(\alpha h\upsilon)^2$ on the photon energy $h\upsilon$ (eV) for polymer electrolytes of different C ratio.

semiconductor increases, causing a blue shift in the UV–Vis absorption spectra due to quantum confinement [31].

Also the indirect optical band gaps E_{gi} were obtained from the linear plots of $(\alpha h\upsilon)^{1/2}$ versus $h\upsilon$ as shown in Fig.(4.20) for all samples, and the values of E_{gi} are summarized in table (4.10).

On the other hand, for optical transitions caused by photons of energy $h\upsilon \prec E_g$, the absorption of photons is related to the presence of localized tail states in the forbidden gap. The width of this tail, called the Urbach tail, is an indicator of the defect levels in the forbidden band gap. Urbach assumed that the absorption coefficient near the band edge shows exponential dependence on photon energy according to the following relation [58]

$$\alpha = \alpha_o \exp(\frac{h\upsilon}{E_u}) \qquad (4.19)$$

where α_o is constant and E_u is the Urbach's energy corresponding to the width of the band tails of the localized states in the band gap. These are formed as a result of extrinsic origins arising from defects or impurities, to extended states in the conduction bands. The values of E_u were estimated using the least square fitting of equation (4.12). Fig.(4.21) shows the relation between $Ln(\alpha)$ versus photon energy $h\upsilon$ for all samples. The extracted values of E_u are listed in table (4.10).

The variation of the magnitude of E_u of polymer electrolytes can be understood by considering the mobility concept that filling significantly affects the Urbach energy E_u as proposed by Davis and Mott [90]. The process of filling introduces additional defect states in the polymeric matrix. The density of localized states was found to be proportional to the concentration of these

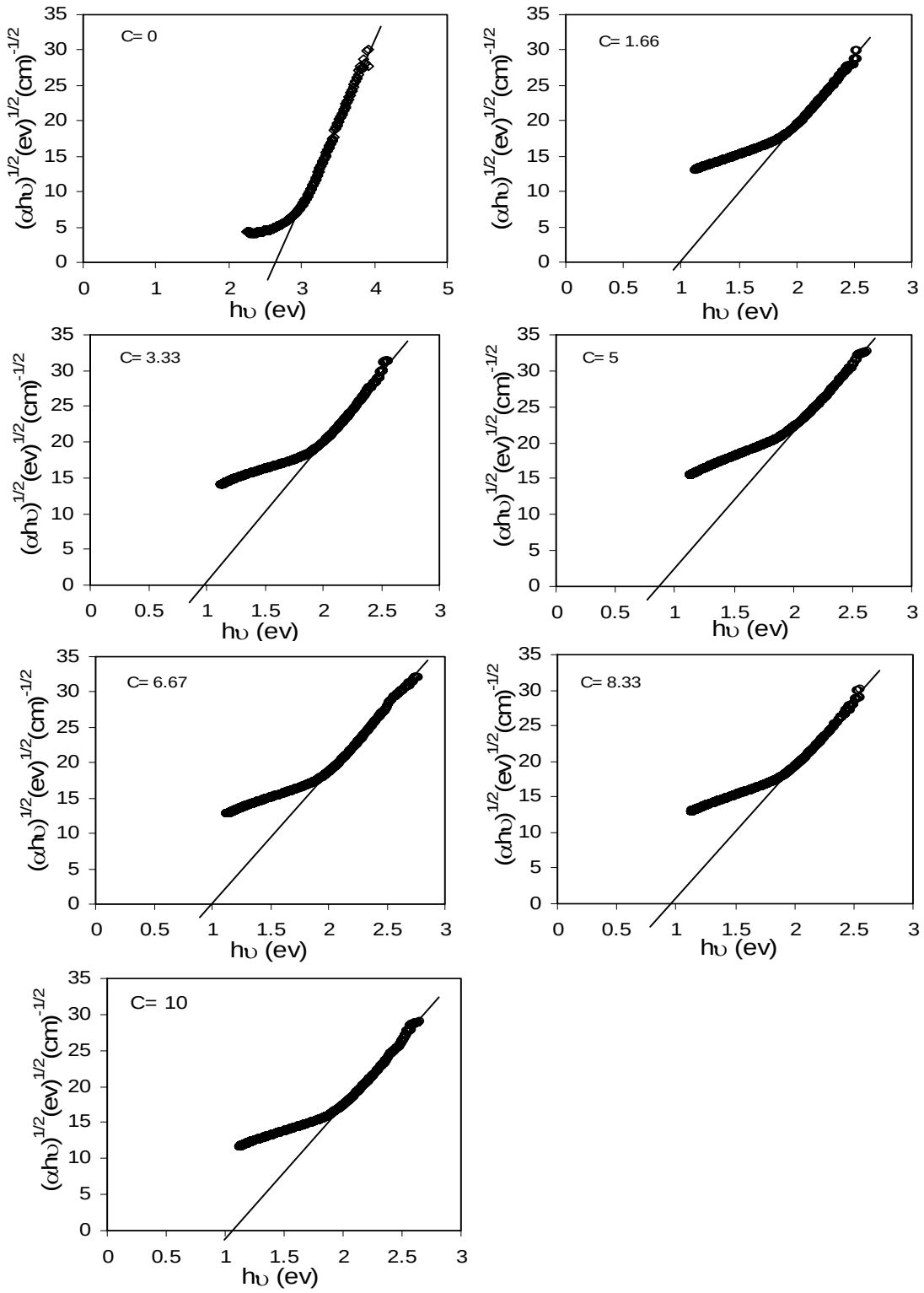

Fig.(4.20): The dependence of $(\alpha h\upsilon)^{1/2}$ on the photon energy $h\upsilon$ (eV) for polymer electrolytes of different C ratio.

Table (4.10): Extracted values of the direct E_{gd} , indirect E_{gi} band gap and Urbach tail E_u for polymer electrolytes of different C (NaI / $CuCl_2$) ratio.

C (NaI / CuCl)	E_u (eV)	E_{gd} (eV) (direct)	E_{gi} (eV) (indirect)
0	0.35	3.39	2.7
1.66	0.89	1.98	1
3.33	0.91	2.048	0.99
5	1.17	1.99	0.82
6.67	0.88	2.14	1
8.33	0.91	2.047	0.95
10	0.84	2.12	1.1

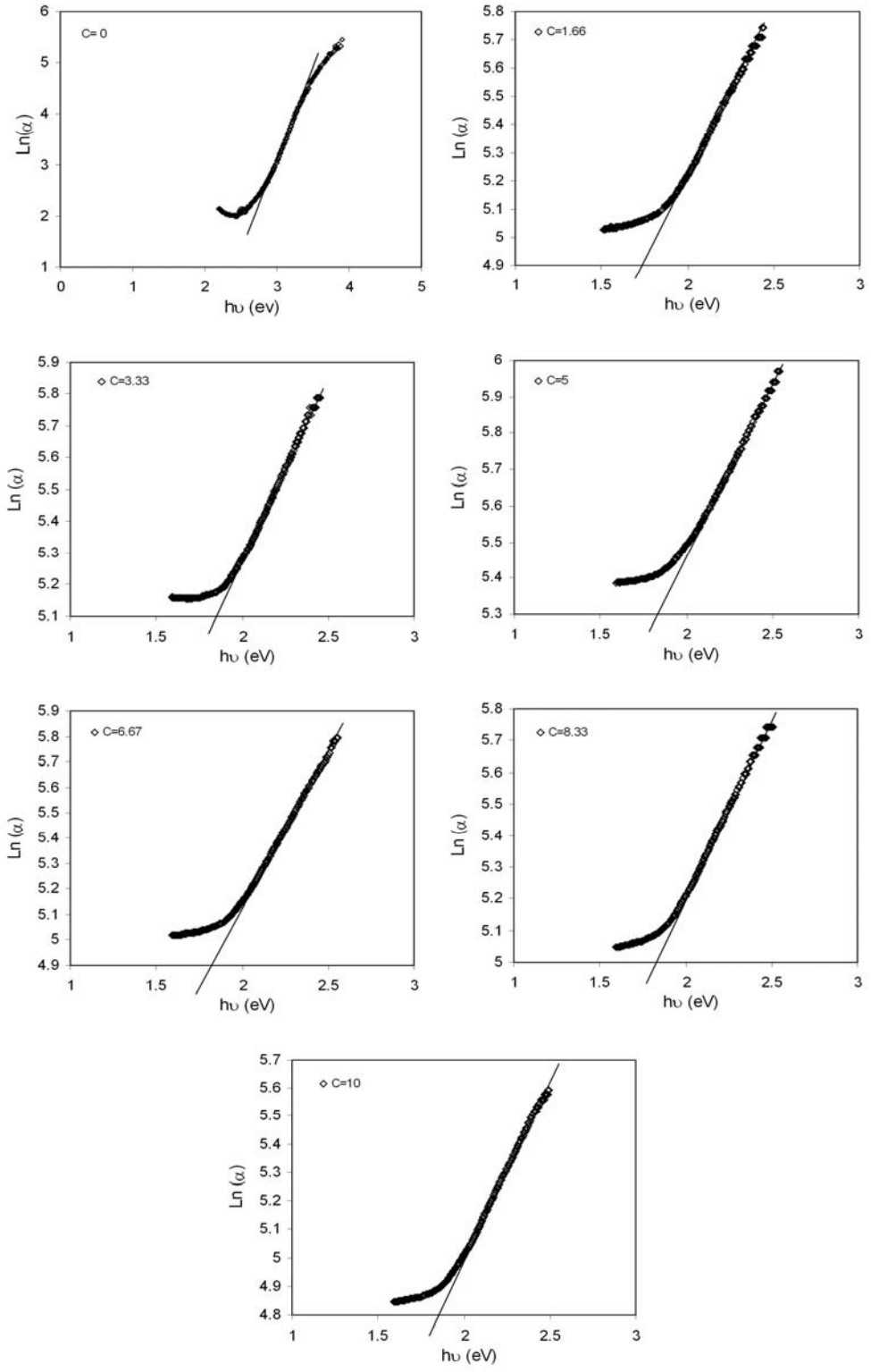

Fig.(4.21): The dependence of $\ln(\alpha)$ on the photon energy $h\upsilon$ (eV) for polymer electrolytes of different C ratio.

defects [58] and consequently to CuI and free iodine contents. The increase of salt ratio content may cause the localized states of different colour centres to overlap and extend in the mobility gap [91]. This overlap may provide evidence of the considerable change in E_u when salt ratio is increased in the polymeric matrix.

The magnitudes of ΔE_b obtained from conductivity data are small in comparison with optical band gap energies E_{gd}. This is due to the fact that their nature is different. While the activation energy corresponds to the energy required for conduction from one site to another, the optical band gap corresponds to interband transition.